Turkish Journal of Electrical Engineering & Computer Sciences

http://journals.tubitak.gov.tr/elektrik/

Research Article

Turk J Elec Eng & Comp Sci
(2016) 24: 384 – 397

doi:10.3906/elk-1307-76

Linear model of a three-phase shunt active power filter with a hysteresis controller

Kadir VARDAR[1,*], **Eyup AKPINAR**[2]

[1]Department of Electrical and Electronics Engineering, Faculty of Engineering, Dumlupınar University, Kütahya, Turkey

[2]Department of Electrical and Electronics Engineering, Faculty of Engineering, Dokuz Eylül University, Buca, İzmir, Turkey

Received: 10.07.2013 • **Accepted/Published Online:** 09.10.2013 • **Final Version:** 05.02.2016

Abstract: In this work, a linear model of a 3-phase active power filter (APF) is obtained to design a DC link proportional–integral (PI) controller. The system is designed on the basis of a TMS320F2812 digital signal processer (DSP). The PI controller is implemented in the program of the DSP. The hysteresis controller and sampling frequency are also taken into account in the linear model. The effect of hysteresis bandwidth, filter inductance, DC link capacitor, and sampling frequency on the stability are investigated by using the Routh–Hurwitz method. The detailed simulation model in MATLAB and experimental results showed that the linear model can be used to specify the PI controller's parameters.

Key words: Active power filters, hysteresis current controller, DC link PI controller, stability

1. Introduction

Shunt active power filters (APFs) have been widely used to compensate the current harmonics of nonlinear loads. A three-phase voltage source AC to DC converter is used with a hysteresis current controller to inject harmonic currents [1–7]. The choice of the current control technique has a crucial role to obtain a desired performance in practical applications. A hysteresis current controller is preferred in many applications because of its simplicity and robustness. The main disadvantages of this controller are the varying switching frequency and unpredicted harmonics related to switching frequency. The hysteresis band in digital implementation may be violated if the sampling frequency is not sufficiently high. The parallel resonance between supply inductance [8,9] and shunt reactive power compensation capacitors can also be observed if the frequency of harmonic currents injected by the APF corresponds to the resonance frequency.

Some analytical methods have been developed for modeling and simulation of APFs [3]. The switching function model enables a fast analysis with computer simulations [10]. The DC model provides a simple harmonic equivalent circuit, but does not cover the mutual couplings between the three phases [11]. It offers an analysis for transient response of the DC link voltage alone. The current controller and DC link proportional–integral (PI) controller are usually analyzed in a synchronously rotating reference frame. The pulse width modulated (PWM) signals are also included in the models by defining the switching functions. Then the direct and quadrature axes' currents are decoupled and controlled separately [12]. The inner (current) and outer loops (DC link voltage) are frequently decoupled from each other to control the DC link voltage and converter input current independently [13,14]. A second-degree characteristic equation is obtained for a closed loop subsystem [13–16] by using a decoupled structure.

*Correspondence: kadir.vardar@dpu.edu.tr

The hysteresis current controller is usually considered a robust controller for PWM converters and it does not require a decoupled transfer function. When this analogue controller is implemented in a digital signal processor (DSP), the execution time and the sampling frequency become key parameters for the success of the controller. If the sampling period and execution time are not small enough, the bandwidth may be avoided and stable operation of the system may not be protected. Therefore, it is crucial to incorporate the sampling period and execution time into the linear model. In this work, the parameters of the digital system such as sampling frequency and execution time of the DSP are taken into consideration. Then the DC link PI parameters are estimated by applying the Routh– Hurwitz criteria.

2. Model of the shunt active power filter

The circuit diagram of a three-phase shunt APF in parallel to a nonlinear load is given in Figure 1. The load current is measured by means of Hall effect current sensors and its harmonic component is extracted by using the instantaneous reactive power method, which is widely used among the other methods reported [4,5]. The compensating currents are injected into the three-phase electrical network at the point of common coupling (PCC). A digital PI controller is programmed in the DSP to regulate the DC bus voltage. The set of differential equations for the three-phase active power filter without a neutral line can be written as follows [12,17]:

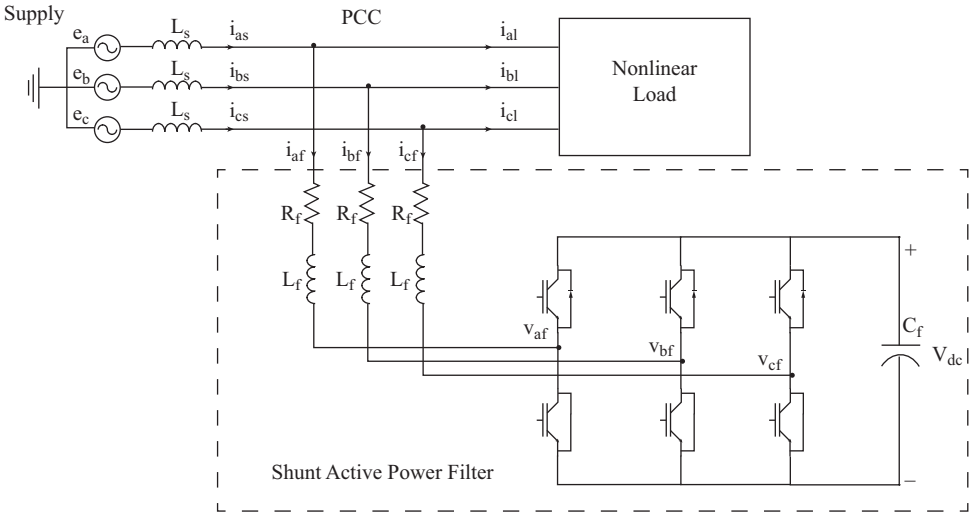

Figure 1. Circuit diagram of APF with a nonlinear load.

$$L_f \frac{d}{dt} i_{af} = e_a - R_f i_{af} - v_{af} \tag{1}$$

$$L_f \frac{d}{dt} i_{bf} = e_b - R_f i_{bf} - v_{bf} \tag{2}$$

$$L_f \frac{d}{dt} i_{cf} = e_c - R_f i_{cf} - v_{cf} \tag{3}$$

$$C_{dc} \frac{d}{dt} v_{dc} = f_a i_{af} + f_b i_{bf} + f_c i_{cf}, \tag{4}$$

where f_a, f_b, and f_c are switching functions. L_f and R_f are filter inductance and its resistance, respectively. C_{dc} is the capacitance at the DC link. Three phase voltages, currents and switching functions in Eqs. (1)–(4) are transformed to a synchronously rotating reference frame by using Eq. (5):

$$\begin{bmatrix} x_q \\ x_d \\ x_0 \end{bmatrix} = \frac{2}{3} \begin{bmatrix} \cos\theta_e & \cos(\theta_e - \frac{2\pi}{3}) & \cos(\theta_e + \frac{2\pi}{3}) \\ \sin\theta_e & \sin(\theta_e - \frac{2\pi}{3}) & \sin(\theta_e + \frac{2\pi}{3}) \\ \frac{1}{2} & \frac{1}{2} & \frac{1}{2} \end{bmatrix} \begin{bmatrix} x_a \\ x_b \\ x_c \end{bmatrix} \tag{5}$$

The sum of the phase currents is zero for three-phase three-wire systems. Therefore,

$$L_f \frac{d}{dt} i^e_{qf} = e_q - R_f i^e_{qf} - \omega_e L_f i^e_{df} - v^e_{qf} \tag{6}$$

$$L_f \frac{d}{dt} i^e_{df} = e_d - R_f i^e_{df} + \omega_e L_f i^e_{qf} - v^e_{df} \tag{7}$$

$$C_{dc} \frac{d}{dt} \nu_{dc} = \frac{3}{2}(f_d i^e_{df} + f_q i^e_{qf}) \tag{8}$$

$$v^e_{qf} = f_q \cdot v_{dc} \tag{9}$$

$$v^e_{df} = f_d \cdot v_{dc} \tag{10}$$

D-axis of the supply voltage is positioned such that it coincides with the positive peak value of phase-a voltage of supply $e_d = V_m$. In this case, the q axis component of the supply voltages will be zero $e_q = 0$. Hence, the direct and quadrature axes' components of reference currents are expressed as follows:

$$i^{e^*}_{df} = i_1 - i^e_{dL} + i_{dc} \tag{11}$$

$$i^{e^*}_{qf} = -i^e_{qL}, \tag{12}$$

where i_{dc} is the output of the DC link voltage PI controller. i^e_{dL} and i^e_{qL} are the components of load current corresponding to real and reactive powers, respectively. The reactive power demand of load is supplied by the grid; therefore, the reference current of the APF does not contain a quadrature component of the load current, $i^{e^*}_{qf} = 0$.

3. Linear model of the APF and hysteresis controller

The simulation of the APF was carried out using the block diagram in Figure 2. The "relay model" in Simulink is used for the hysteresis operation. The error and switching functions at the synchronously rotating reference frame are obtained and given in Figure 3. The results show that the d-axis component of error varies between $\pm$ HB, while the average value of f_d is almost constant and its magnitude is equal to V_m / V_{dc}. The ripples on f_d can be resolved into two components. One of them is created by ε_d forcing f_d to be zero during the time when ε_d violates the upper limit of the hysteresis band. When ε_d violates the lower limit of the hysteresis band,

then f_d will be equal to V_m / V_{dc}. The other ripple component is created by ε_q and has a sawtooth waveform. The switching function on the d-axis f_d can be expressed as follows when the effect of ε_q is neglected:

$$f_d = \frac{V_m}{V_{dc}} \cdot f_a(\varepsilon_d, HB) \tag{13}$$

The model of the converter is established on the basis that the q-axis component of the supply voltage and filter current are both zero ($e_q = 0$ and $i_{qf}^{e^*} = 0$). By neglecting the voltage drop on the inductance at the fundamental frequency, the average value of v_{qf}^e is zero; hence f_q is zero from Eq. (9).

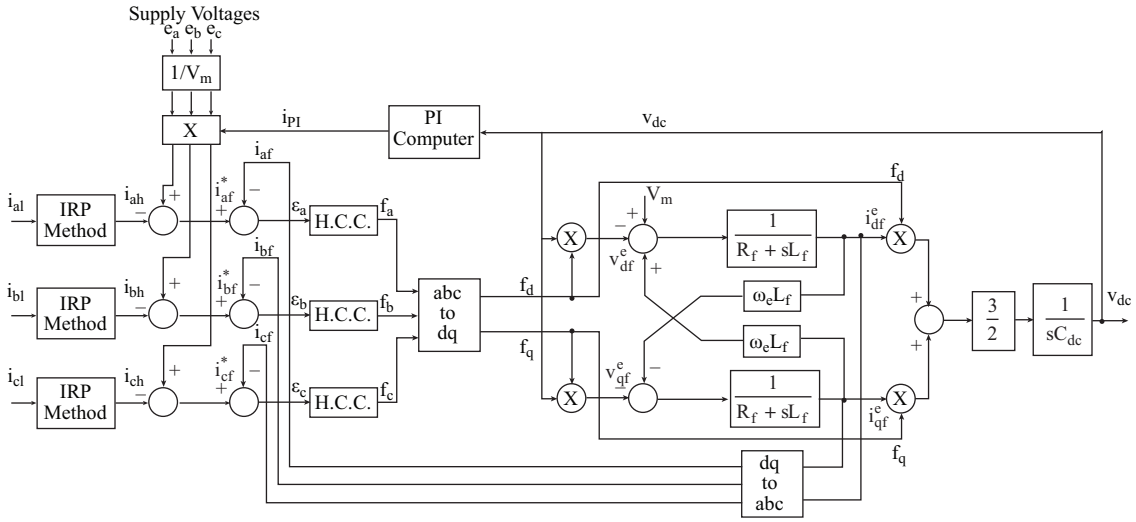

Figure 2. The block diagram of shunt active power filters at SRF.

The hysteresis effect links the error to the f_d component and the block diagram of the APF is reconstructed by taking this analysis into consideration as shown in Figure 4. The hysteresis loop is linearized between the two switching intervals as shown in Figure 5. Hence,

$$f_a(\varepsilon_d, HB) = \frac{HB - \varepsilon_d}{2 \cdot HB} \tag{14}$$

Two multiplication units in Figure 4 are replaced by two summation blocks as shown in Figures 6a–6d by assuming that $V_{dc}(t)$ is equal to V_{dc}^* and $f_d(t)$is equal to F_d at the steady-state operation of the system [16]. The block diagram is modified after these linearizations and it is given in Figure 7.

The analysis of this linear model is carried out in MATLAB with the parameters given in the Appendix and the results are verified by the detailed simulation model given in Figure 2. The variation in the DC link voltage and the reference filter current from both models are given in Figures 8a and 8b. Neglecting the effect of f_q in the linear model created a small change in the settling time of the capacitor voltage.

4. Design of DC link PI controller

The model was obtained in terms of the sampling frequency, band width, and execution time. The switching frequency changes due to the level of DC link voltage, switching filter inductance, band width, and rate of

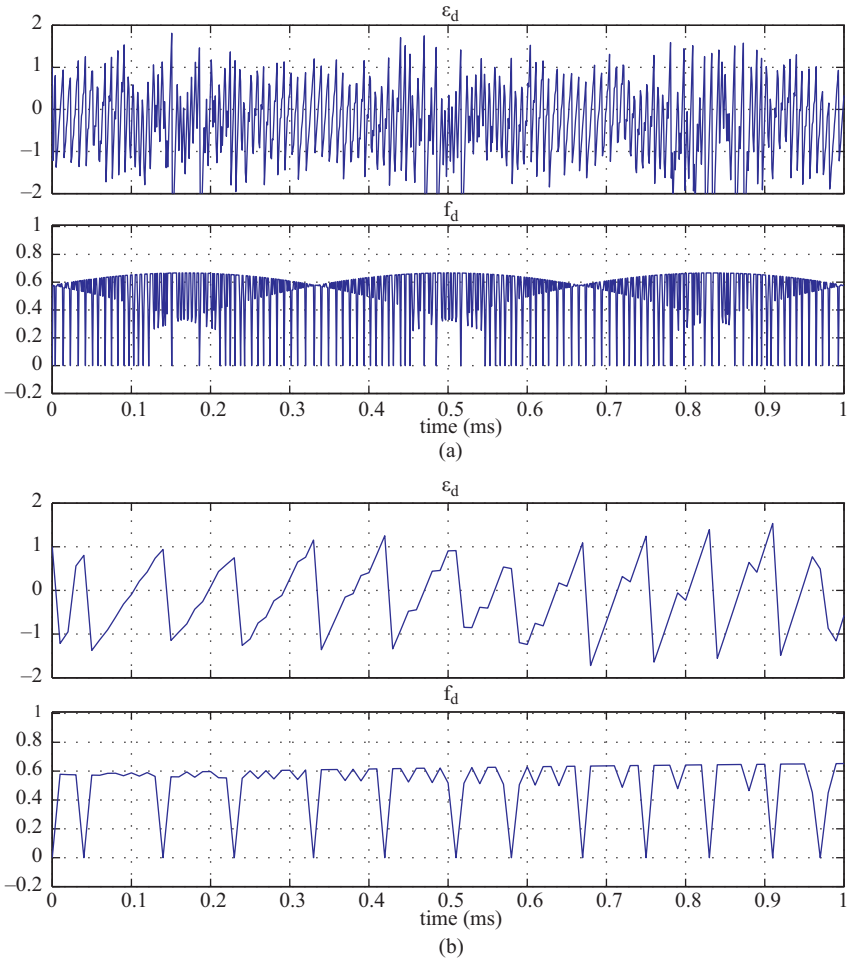

Figure 3. The d axis switching functions and the reference current errors: (a) During half of the fundamental supply frequency. (b) Expanded waveforms for high resolution.

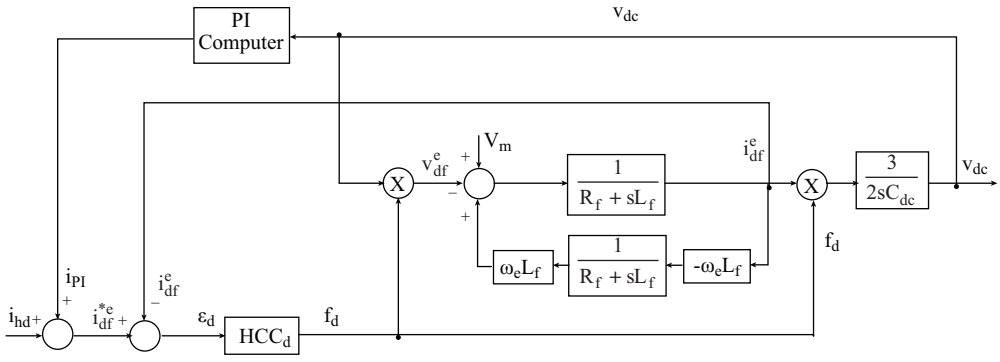

Figure 4. Block diagram of active power filter on d axis.

change of the reference current. The error between the reference and actual DC link voltages is passed through a digital PI controller programmed in the DSP.

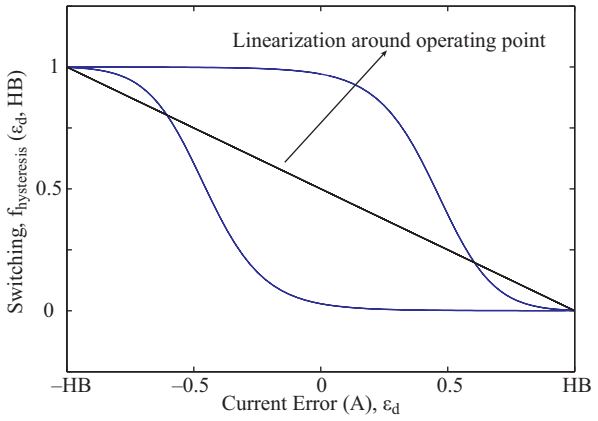

Figure 5. Linearization of hysteresis band.

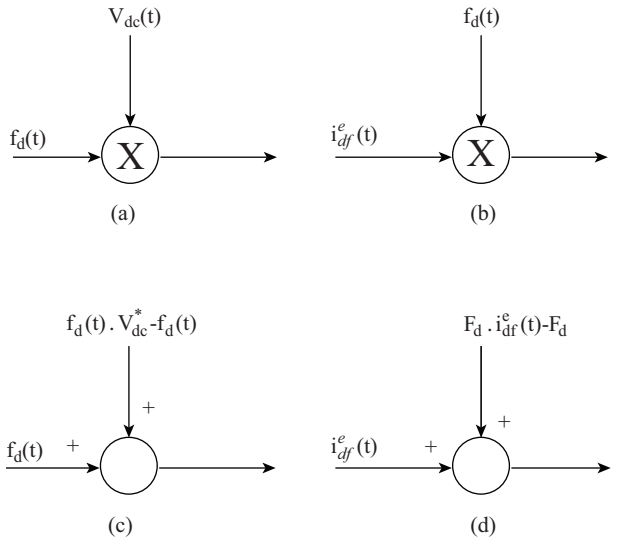

Figure 6. Multiplication blocks converted to summation: (a) the product block for $V_{dc}(t)$ input, (b) the product block for $f_d(t)$ input, (c) converted block for $V_{dc}(t)$ input at the steady state, (d) converted block for $f_d(t)$ input at the steady state.

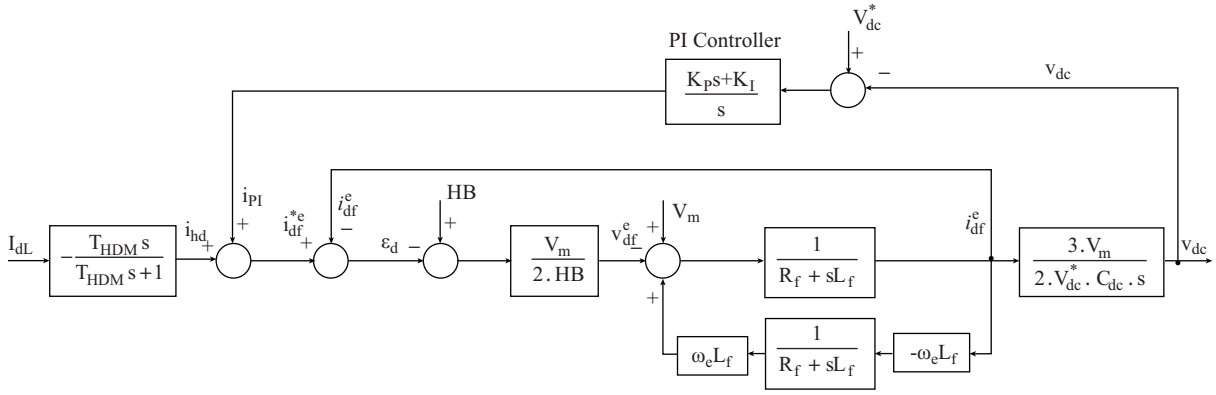

Figure 7. Block diagram of linearized system.

The change in output of the PI controller is expressed in terms of error, change of error, and sampling time (T_S) as follows [18]:

$$\Delta u(n \cdot T_S) = K_{CE} \cdot \Delta\varepsilon(n \cdot T_S) + K_E \cdot \varepsilon(n \cdot T_S), \tag{15}$$

where

$$K_{CE} = K_P \text{ and } K_E = K_i \cdot T_S \tag{16}$$

The software in the DSP is a time-consuming program because of digital filters and transformations. The execution time of the program specifies the sampling time, switching frequency, and alleviation of harmonic

currents. A complete cycle between the sampling and switching of the DC link capacitor voltage is represented by a time delay of T_s. A low-pass filter with the time constant T_s is located between the reference and measured DC link voltage for this purpose as shown in Figure 9.

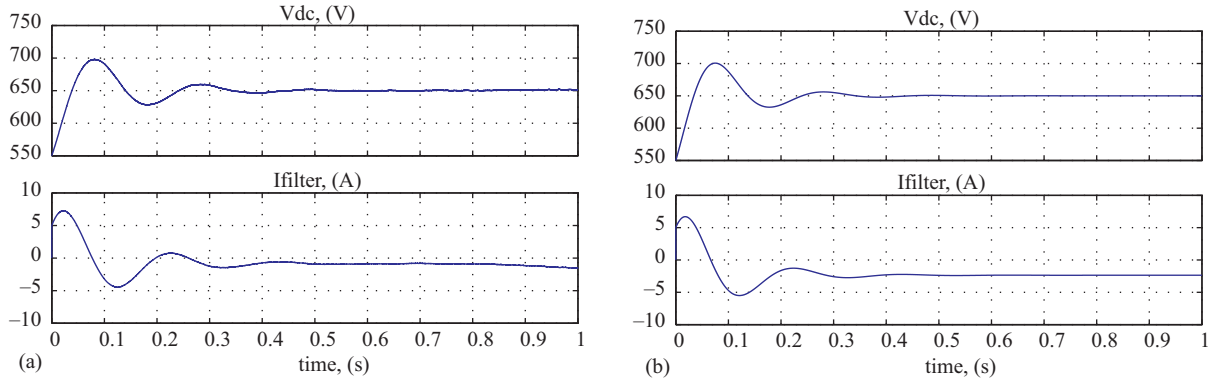

Figure 8. Simulation results with HB = 4 A: (a) SRF model (b) linearized model.

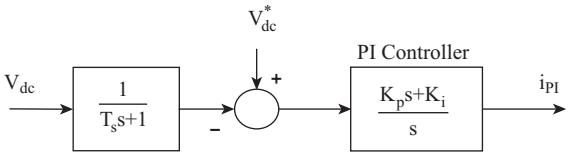

Figure 9. Low-pass filter representing the execution time.

The linear relation between the direct axis converter input voltage and the error signal ε_d is obtained by using Eqs. (10) and (14) as follows:

$$v_{df} \cong f_d \cdot V_{dc}^* = \frac{V_m \cdot (HB - \varepsilon_d)}{2 \cdot HB} \tag{17}$$

The reference DC link voltage V_{dc}^* and peak supply voltage V_m are kept constant during the operation. The transfer function between the capacitor voltage and direct axis component of load current can also be obtained as follows from the blocks in Figure 7.

$$\frac{\Delta V_{dc}(s)}{\Delta I_{dL}(s)} = \frac{-3 \cdot V_m^2 \cdot T_{HDM} \cdot (1 + T_s \cdot s) \cdot s^2}{(T_{HDM} \cdot s + 1) \cdot \Delta(s)} \tag{18}$$

The resistance of the switching inductor R_f is neglected for simplicity of the transfer functions here, but it is a damping parameter for DC link voltage transients. Therefore, this resistance ($R_f = 0.2$ ohms) is included in the analysis in MATLAB.

The characteristic equation and its coefficients are obtained as follows:

$$\Delta(s) = b_4 \cdot s^4 + b_3 \cdot s^3 + b_2 \cdot s^2 + b_1 \cdot s + b_0 \tag{19}$$

$$b_4 = 4 \cdot HB \cdot L_f \cdot V_{dc}^* \cdot C_{dc} \cdot T_s$$

$$b_3 = 4 \cdot HB \cdot L_f \cdot V_{dc}^* \cdot C_{dc} + 2 \cdot V_m \cdot V_{dc}^* \cdot C_{dc} \cdot T_s$$

$$b_2 = 2 \cdot V_m \cdot V_{dc}^* \cdot C_{dc} + 4 \cdot \omega_e^2 \cdot HB \cdot L_f \cdot V_{dc}^* \cdot C_{dc} \cdot T_s$$

$$b_1 = 4 \cdot \omega_e^2 \cdot HB \cdot L_f \cdot V_{dc}^* \cdot C_{dc} + 3 \cdot V_m^2 \cdot K_p$$

$$b_0 = 3 \cdot V_m^2 \cdot K_i$$

The stability is guaranteed if the transfer function does not have any poles in the right half plane. The stable operating region of the DC link voltage PI controller is specified by applying the Routh–Hurwitz method [19]. Hence the following three constraints are taken into consideration:

i)

$$3 \cdot V_m^2 \cdot K_i > 0 \Rightarrow K_i > 0 \tag{20}$$

ii) $4 \cdot \omega_e^2 \cdot HB \cdot L_f \cdot V_{dc}^* \cdot C_{dc} + 3 \cdot V_m^2 \cdot K_p > 0$

$$\Rightarrow K_p > -\frac{4 \cdot \omega_e^2 \cdot HB \cdot L_f \cdot V_{dc}^* \cdot C_{dc}}{3 \cdot V_m^2} \tag{21}$$

The entries of the Routh array are formed from the coefficients of the characteristic equation in the s-domain in Eq. (19).

s^4	s^3	s^2	s^1	s^0
b_4	b_3	$b_2 - b_4 b_1 / b_3$	$b_1 - \left(\frac{b_3 b_0}{b_2 - (b_4 b_1 / b_3)}\right)$	b_0

(22)

For a given set of variables, their effect on stability can be checked by evaluating the sign. Each column of the Routh array must be positive and not changing sign for stable operation.

iii)

$$b_1 - \left(\frac{b_3 b_0}{b_2 - (b_4 b_1 / b_3)}\right) > 0 \tag{23}$$

The ranges of K_{CE} and K_E parameters are determined for stable operation and are shown in Figures 10a–10d. In order to determine the change in roots, the root locus graphs are also plotted and given in Figures 11a–11d. The K_{CE} and K_E parameters of the PI controller are associated with each other in different conditions and K gain is defined in relation to them. The root locus plots verified the results of the Routh–Hurwitz method given in Figure 10.

The relations between direct axis components of the load current, filter current, and harmonic current are obtained by using the block diagram in Figure 7 as follows:

$$\frac{\Delta i_d(s)}{\Delta I_{dL}(s)} = \frac{-2 \cdot V_m \cdot V_{dc}^* \cdot C_{dc} \cdot T_{HDM} \cdot (1 + T_s \cdot s) \cdot s^3}{(T_{HDM} \cdot s + 1) \cdot \Delta(s)} \tag{24}$$

$$\frac{\Delta i_d(s)}{\Delta i_{hd}(s)} = \frac{2 \cdot V_m \cdot V_{dc}^* \cdot C_{dc} (1 + T_s \cdot s) \cdot s^2}{\Delta(s)} \tag{25}$$

Figures 12a and 12b show the Bode diagrams of Eqs. (24) and (25), respectively. The gain is almost constant between 100 rad/s and 10,000 rad/s. The phase difference is zero between the reference current and filter

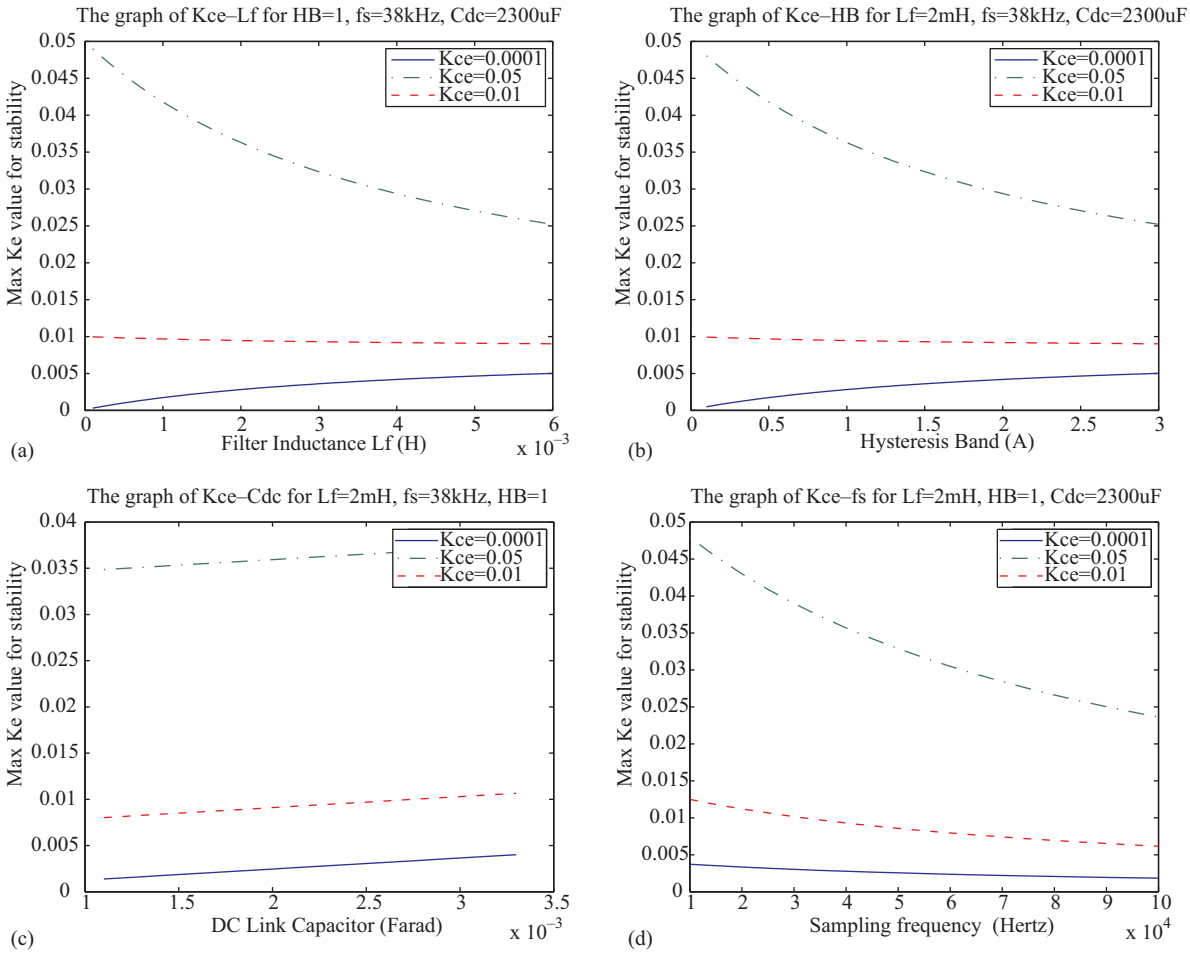

Figure 10. Stability range of DC link PI controller parameters with respect to system parameters. According to the change in: (a) filter inductance, (b) hysteresis band, (c) DC link capacitor, (d) sampling frequency.

current during this interval. There is a 180 degree phase shift between the load current and filter current for harmonic compensation. Figure 12b shows that the gain between filter current and current harmonics of the load is greater than zero dB around 100 rad/s. The PI controller does not keep the DC link voltage constant around this frequency and there is a periodical oscillation around the reference DC link voltage. This periodical oscillation is verified by the results of the detailed simulation program in MATLAB-Simulink.

5. Experimental results

The load current, supply current, and DC link voltage are also recorded during the starting period and steady-state operation of a prototype 20 kVA APF controlled by a TMS320F2812 DSP. The reference current extraction method and hysteresis current controller are operated as two independent tasks in the DSP. The value of reference current is updated with the main program cycle $T_s = T_{HDM} = 38$ kHz, while the hysteresis current controller updates the switching signals around 100 kHz in an interrupt service routine. The performance of method depends on phase error, frequency, and transient responses of the digital filter. A 10th order Butterworth LPF was designed by using the Filter Design Toolbox in MATLAB. The cut-off frequency of the filter was chosen as 100 Hz with a sampling frequency of 38 kHz. The execution time of all routines in the program is 24.94 μs.

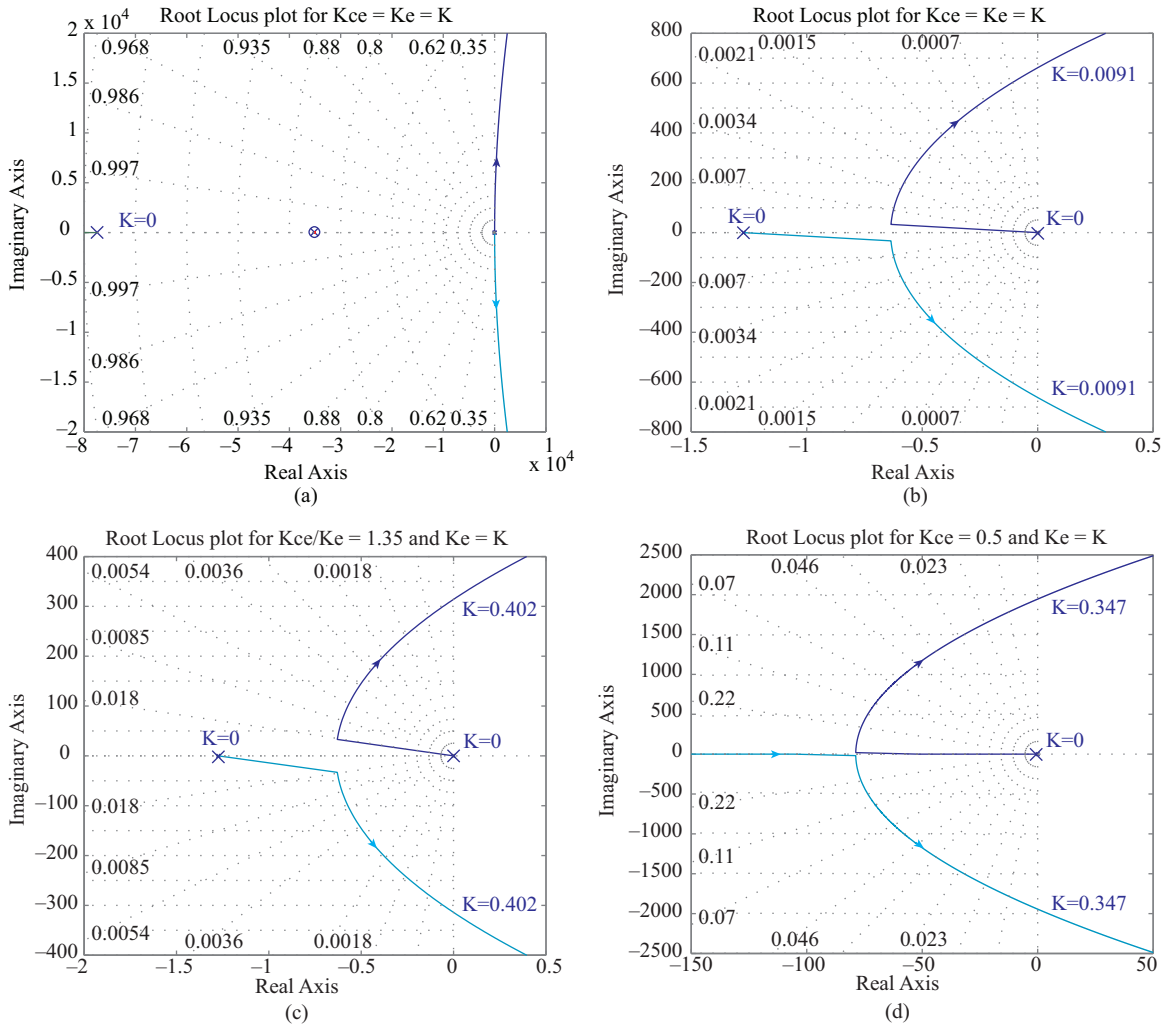

Figure 11. Root locus plots of system. According to the change in K gain: (a) for $K_{CE} = K_E = K$, (b) zoom in for $K_{CE} = K_E = K$, (c) for $K_{CE}/K_E = 1.35$ and $K_E = K$, (d) for $K_{CE} = 0.5$ and $K_E = K$.

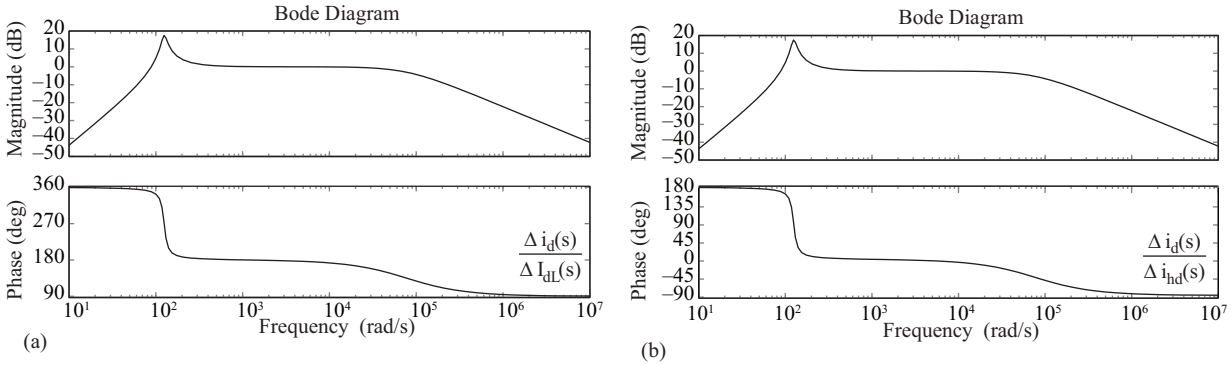

Figure 12. Gain and phase variations according to frequency: (a) for Eq. (24), (b) for Eq. (25).

The load consists of a three-phase diode bridge rectifier in parallel with a three-phase resistive load. The DC link capacitor is charged at the beginning by the three-phase uncontrolled rectifier built in the voltage source converter. The APF is operated when the simulation time is equal to 0.3 s and the load draws 20 A. The reference DC link voltage was set to 650 V; therefore, the capacitor voltage is boosted from the output voltage of the three-phase uncontrolled rectifier to the set value under the PI and hysteresis current controllers. The measurements are obtained with a 400 MHz oscilloscope (LeCroy 604Zi), its ADP305 differential voltage, and AP015 current probes. The load current, supply current, and DC link voltage waveforms from the detailed simulation program are given in Figure 13a and their measured values are given in Figure 13b. The DC link voltage rises to 700 V with an overshoot and settles down to the reference value (650 V) when the simulation time is around 0.8 s. The DC link voltage is recorded with 650 V DC offset.

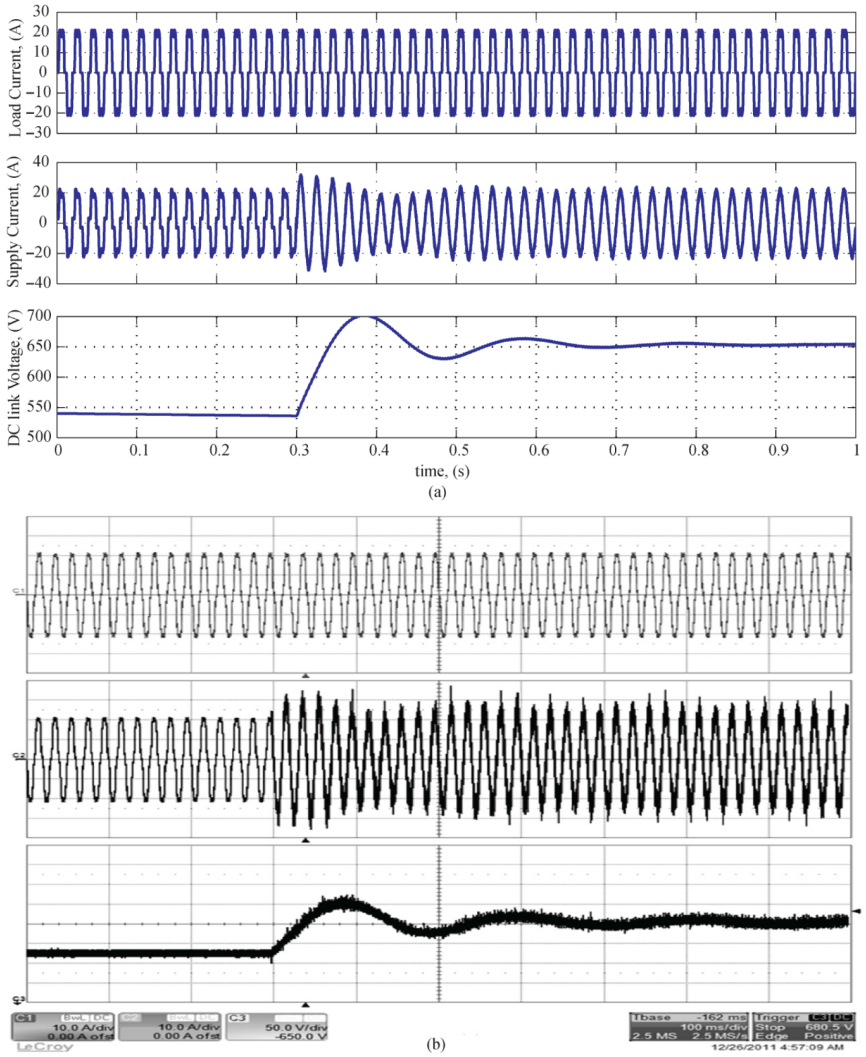

Figure 13. Transient response of shunt active power filter at the start: (a) results from MATLAB model, (b) measured results.

When the experimental and detailed simulation results given in Figures 13a and 13b are compared to the results obtained from the linear model and given in Figure 8, they are compatible during the starting period. The different parts of the system designed in the laboratory are given in Figures 14a–14g.

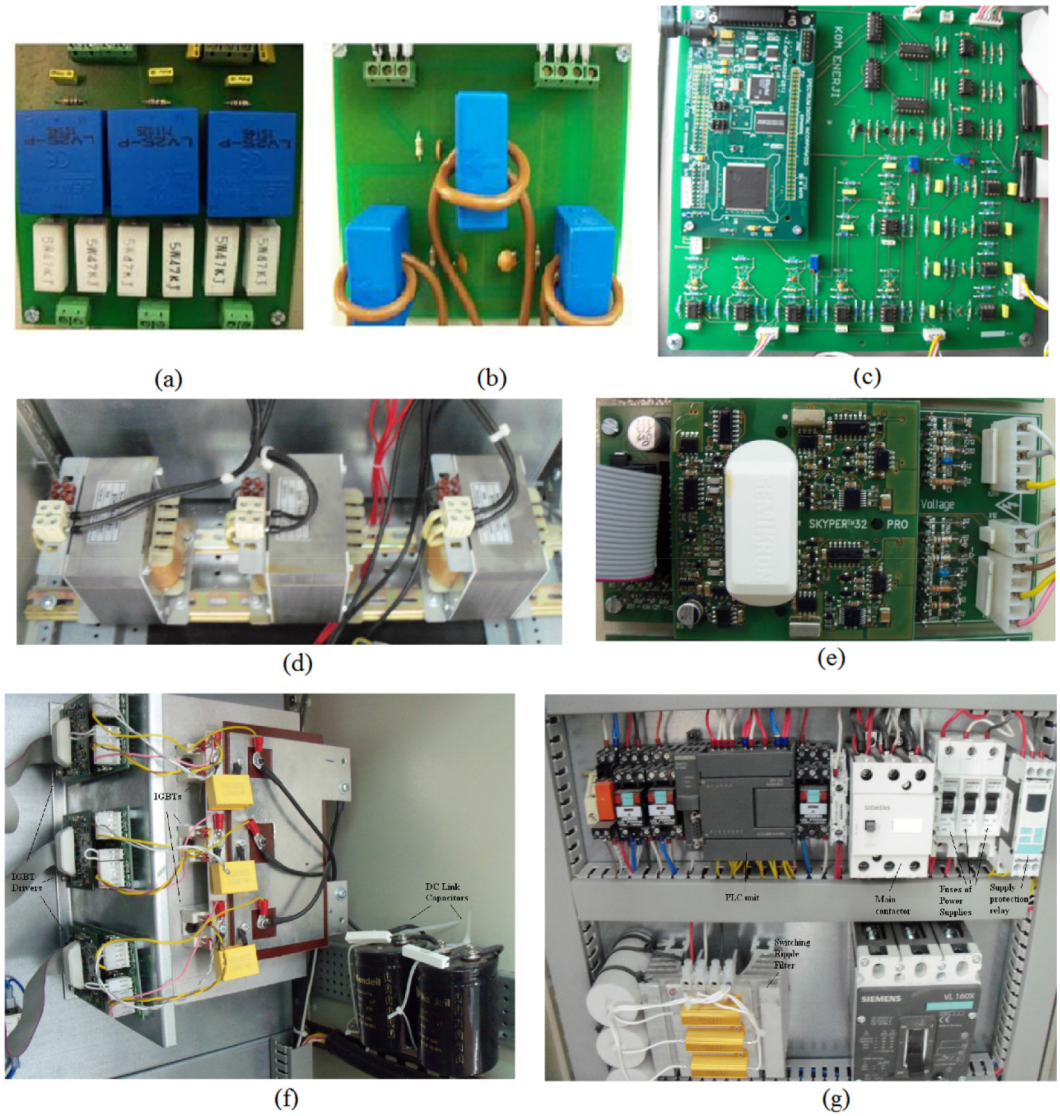

Figure 14. The parts of designed test system: (a) Voltage measurement card, (b) Current measurement card, (c) DSP and main control card, (d) Filter Inductances, (e) The drivers of power module, (f) The circuit of power module and drivers, (g) PLC control unit.

6. Conclusions

In this paper, a linear model of a shunt APF that contains a hysteresis current controller is obtained by using a synchronously rotating reference frame. The switching frequency is left as a variable in the d-axis model even though the reference frame speed is selected at the fundamental frequency. This seems to be a reasonable assumption during this linearization because switching frequency is very high with respect to power frequency. The sampling frequency, hysteresis bandwidth, and execution time of the DSP are included in the linear model of a shunt APF. The stability range of a DC link PI controller is found by applying the Routh–Hurwitz criteria. The transfer functions between the load current and filter current are obtained and the Bode plots are given. The linear model used here has a fourth-degree characteristic equation. It should be noted that the decoupled

controllers on the direct and quadratic axes reduce the degree of characteristic equation to two. The experimental records showed that linear model of the APF can be successfully used to design the dc link PI controller.

Symbol list

L_f	switching inductance
L_s	source inductance
R_f	resistance of switching inductor
R_s	source resistance
C_{dc}	DC link capacitor
e_a, e_b, e_c	supply voltages
v_{af}, v_{bf}, v_{cf}	terminal voltages of active power filter
i_{af}, i_{bf}, i_{cf}	filter currents
i_{al}, i_{bl}, i_{cl}	load currents
i_{ah}, i_{bh}, i_{ch}	harmonic currents from generated by load
f_a, f_b, f_c	switching functions of each phase
f_d, f_q	d, q components of switching functions
F_d, F_q	simplifying on f_d, f_q
i^e_{df}, i^e_{qf}	d, q components of filter currents in SRF
$i^{e\prime}_{df}$	decomposed d axis current of filter
$i^{e^*}_{df}, i^{e^*}_{qf}$	reference currents in SRF
i^e_{dL}, i^e_{qL}	d, q components of load current
v^e_{df}, v^e_{qf}	d, q components of terminal voltages
i_{dc}	DC link current
ω_e	Synchronously angular velocity
HB	hysteresis band
$\varepsilon_a, \varepsilon_b, \varepsilon_c$	The current tracking errors of each phase
c	shape parameter of hysteresis function
α	scaling parameter of hysteresis function
ε_{PI}	PI controller error
ε_i	current error of decomposed current
v_{dc}, v^*_{dc}	DC link actual and reference voltages
v_m	peak voltage of supply
K_p , K_i	proportional and integral gains
K_E, K_{CE}	proportional and integral gains of digital PI controller

References

[1] Akagi H. Trends in active power line conditioners. IEEE T Power Electr 1994; 9: 263-268.

[2] Akagi H. New trends in active filters for power conditioning. IEEE T Ind Appl 1996; 32: 1312-1322.

[3] Emadi A, Nasiri A, Bekiarov SB, Uninterruptible Power Supplies and Active Filters. Boca Raton, FL, USA: CRC Press, 2005. pp. 63-111.

[4] Vardar K, Surgevil T, Akpinar E. Evaluation of reference current extraction methods for DSP implementation in active power filters. Elec Power Sys Res 2009; 79: 1342-1352.

[5] Vardar K, Akpinar E. Comparing ADALINE and IRPT methods based on shunt active power filters. Eur T Electr Power 2011; 21: 924-936.

[6] Uçar M, Özdemir Ş, Özdemir E. A unified series-parallel active filter system for nonperiodic disturbances. Turk J Elec Eng & Comp Sci 2011; 19: 575-596.

[7] Alışkan İ, Gülez K, Altun Y. Spoiler effects reduction with using active power filter on a direct torque controlled induction machine. Turk J Elec Eng & Comp Sci 2011; 19: 787-796.

[8] Buso S, Malesani L, Mattavelli P. Comparison of current control techniques for active filter applications. IEEE T Ind Electr 1998; 45: 722-729.

[9] Li C, Tan Y. A hybrid neural network based modeling for hysteresis. In: IEEE 2005 Proceedings of the IEEE Int Symposium on Intelligent Control; 27-29 June 2005; Limassol, Cyprus: IEEE. pp. 53-58.

[10] Lee BK, Ehsani M. A simplified functional simulation model for 3-phase voltage-source inverter using switching function concept. IEEE T Ind Electr 2001; 48: 309-321.

[11] Srianthumrong S, Akagi H. A DC model for transient analysis of a series active filter integrated with double-series diode rectifier. IEEE T Ind Appl 2003; 39: 864-872.

[12] Kuo HH, Yeh SN, Hwang JC. Novel analytical model for design and implementation of three-phase active power filter controller. IEE Proc-B 2001; 148: 369-383.

[13] Mendalek N, Al-Haddad K, Dessaint LA, Fnaiech F. Nonlinear control technique to enhance dynamic performance of a shunt active power filter. IEE Proc-Electr Power Appl 2003; 150: 373-379.

[14] Rahmani S. Mendalek N. Al-Haddad K. Experimental design of a nonlinear control technique for three-phase shunt active power filter. IEEE T Ind Electr 2010; 57: 3364-3375.

[15] Mendalek N, Al-Haddad K. Modeling and nonlinear control of shunt active power filter in the synchronous reference frame. In: IEEE 2000 9th Int. Conf. Harmonics Qual. Power; 1–4 October 2000; Orlando, Florida, USA: IEEE. pp. 30-35.

[16] Li C, Guo B, Li N. The research on stability of deadbeat current control in shunt active power filter. In: IEEE 2009 International Power Electronics and Motion Control Conference; 17–20 May 2009; Wuhan, China: IEEE. pp. 2382-2387.

[17] Blasko V, Kaura V. A new mathematical model and control of a three-phase AC–DC voltage source converter. IEEE T Power Electr 1997; 12: 116-123.

[18] Dote Y, Kinoshita S. Brushless servomotors: fundamentals and applications. Oxford, UK: Clarendon, 1990.

[19] Kuo BC. Automatic Control Systems. 5th ed., Upper Saddle River, NJ, USA: Prentice-Hall, 1987. pp. 354-362.

Appendix

System parameters: $L_f = 1.8$ mH, $R_f = 0.2$ ohms, $C_{dc} = 2300$ μF, $\omega_e = 314$ rad/s,

$v_m = 310$ V, $v_{dc}^* = 650$ V, $K_E = 0.0001$, $K_{CE} = 0.05$, $T_s = T_{HDM} = 38$ kHz.

Load parameters: Three phase rectifier load $R_{dc\_load} = 50$ ohms + Star connected parallel resistive load $R_{load} = 20$ ohms.